Astron. Astrophys. 332, 291–299 (1998)

ASTRONOMY
AND
ASTROPHYSICS

Optical properties of carbonaceous dust analogues

C. Jäger, H. Mutschke, and Th. Henning

Friedrich-Schiller-Universität Jena, Astrophysikalisches Institut und Universitäts-Sternwarte, Schillergässchen 3, D-07745 Jena, Germany

Received 18 September 1997 / Accepted 27 November 1997

Abstract. Structurally different carbon materials with an increasing sp^2/sp^3 ratio were synthesized by pyrolizing cellulose materials at 400, 600, 800 and 1000 °C . The hybridization ratios and the internal structures in these samples were determined by using High Resolution Transmission Electron Microscopy, Electron Energy Loss Spectroscopy, Raman spectroscopy, IR spectroscopy and elemental combustion analysis. The pyrolized carbon samples were embedded in an epoxide resin and the surface was grinded and polished. The reflectance of the samples could be measured in the range between 200 nm and 500 μm, covering most of the spectral range relevant for radiative transfer calculations. Using the Lorentz-oszillator fit method we were able to determine the optical constants n and k. A big change in the optical behaviour could be seen between 600 and 800 °C, which is caused by the presence of free charge carriers in the samples pyrolized at 800 and 1000 °C. In these samples the graphitic areas have been grown to about 1.5 nm in size. The absorption behaviours of small spheres in the Rayleigh limit and a continous distribution of ellipsoids (CDE) were calculated. The spectral index β in the FIR region ($\lambda \geq 100$ μm) increases from 1.2 for the very disordered still aliphatic-dominated carbon material pyrolized at 400 °C to 2.2 for the more ordered graphitic sample carbonized at 1000 °C in case of spherical particles. In the more graphitic samples pyrolized at 800 and 1000 °C, the spectral index β is strongly dependent on the shape of the particles.

Key words: circumstellar matter – dust, extinction – infrared: ISM: lines and bands

1. Introduction

The far-infrared emission of the circumstellar environment of carbon-rich stars and dense molecular cloud cores is believed to be dominated by the emissivity of carbon dust which is assumed to occur in the graphite modification in many dust models (Draine & Lee 1984; Li & Greenberg 1997). A number of reasons, however, contradict the presence of graphite. The far-infrared data of late-type stars generally show a dust emissivity law of $Q(\lambda) \sim \lambda^{-\beta}$ with a spectral index $\beta \approx 1$ (Campbell et al. 1976; Sopka et al. 1985; Martin & Rogers 1987; Gürtler et al. 1996). Furthermore, radiative transfer calculations of envelopes around YSOs showed that a slope of the far-infrared emission proportional to λ^{-2} as expected for graphite grains cannot explain the measured fluxes above a wavelength of 100 μm (Preibisch et al. 1993; Henning et al. 1995). A λ^{-1} behaviour can be expected in a very disordered two-dimensional material like amorphous carbon (Kittel 1963). The FIR-mm grain opacity is the base for the evaluation of important astrophysical parameters like dust temperature, mass loss rates of evolved stars and the estimation of the total dust mass in circumstellar shells or in molecular clouds. The accuracy of our knowledge of the grain opacity determines the precision of these measurements.

For carbon, the possibilities to form solid structures are extremely manifold because of its ability to occur in different hybridization states. Carbon atoms in the sp^3 hybridization state build up a diamond structure, whereas sp^2 hybridized carbon atoms form planar stuctures (graphite). Apart from the distinct hybridization states there exist mixed hybridization states which build up curved structures, in the perfect form these are closed shells (fullerenes). In solid carbon materials, all kinds of mixtures of, for instance, sp^2 and sp^3 hybridization and also mixed hybridization are possible. Moreover, this opens the possibility to consider (and produce) materials of different short-, medium-, and long-range order. Amorphous structures with heavily disturbed graphitic zones and larger contents of sp^3 hybridized carbon are expected to produce spectral indices smaller than 2 in the submillimeter spectral range. Therefore, it is essential to understand the correlation of structural properties and far-infrared optical behaviour of the carbon materials.

We should stress that the FIR-behaviour is not only influenced by the internal structure, but also by the morphology of the carbon grains. It is well known, that the clustering of carbon grains decreases the spectral index β very strongly (Stognienko et al. 1995; Michel et al. 1996).

The influence of the internal structure on the far-infrared behaviour of different carbon materials was already investigated (Koike et al. 1995; Menella et al. 1995; Papoular et al. 1996). The former measurements were done in transmission using polyethylene pellets. This method cannot exactly sepa-

Send offprint requests to: C. Jäger

rate between structural and morphological effects on the FIR absorption.

The absorption behaviour of spheres and a continuous distribution of ellipsoids can be calculated from the optical constants of the carbon material (Bohren & Huffman 1983). Optical data were published so far for graphite and graphite-like materials like glassy carbon or soot materials (Draine & Lee 1984; Edoh 1983; Rouleau & Martin 1991; Zubko et al. 1996).

The aim of this work is on one hand to study synthetic carbon materials with different sp^2/sp^3 ratios and structural order and on the other hand the evaluation of optical constants. For this purpose, pyrolysis of an organic precursor offers the possibility to stop the carbonization at different states representing different sp^2/sp^3 ratios and to obtain the material in bulk form which is important for the determination of the optical constants by reflection spectroscopy.

Because of the very complex structure of carbon materials, they have to be analyzed by different methods. The most important of them are imaging (High Resolution Transmission Electron Microscopy, HRTEM) and spectroscopic methods (infrared, Raman, Electron Energy Loss Spectroscopy, EELS) as well as the determination of the elemental composition. For these well-characterized materials, the complex refractive index was determined from specular reflectance measurements in the spectral range from the UV to submillimeter wavelengths. From the optical constants the FIR behaviour of carbon grains can be calculated taking into account different grain morphologies.

2. Chemical reactions during pyrolysis

As the starting material for the pyrolysis we used the cellulose Avicel pH-101 (Fa. Fluka) with a microcrystallite size of about 50 μm. The precursor was pressed to pellets of about 60 mg mass at a pressure of 2 tons load per 1.3 cm^2. The pellets were placed in a well evacuated quartz-tube flushed with Ar gas. At the beginning of the pyrolysis procedure the samples were outgassed at a pressure of 0.01 mbar for 3 hours at room temperature to remove water and some volatile compounds adsorbed at the surface of the cellulose. The outgassed pellets were heated at a rate of 180 K/h and were kept 2h at the reaction temperature. Afterwards, they were cooled down to room temperature at the same rate of 180 K/h. All steps of pyrolysis including the cooling process were performed under Ar atmosphere at normal pressure. The volume loss of the carbonized pellets was 50–80 % depending on the reaction temperature. The small heating and cooling rates prevented the curvature of the sample which enabled the embedding in an epoxide resin and to grind and polish the surface for reflection measurements.

The chemical reactions and degradation taking place during the carbonization of cellulose material have already been described (Tang & Bacon 1964; Otani & Oya 1991). The first step is a dehydration reaction where ketonic groups are incorporated in the still existing ring structure of the cellulose compound. The glycosidic bonds are destroyed at temperatures between 300 and 400 ^{o}C and CO, CO_2, and H_2O are released. The resulting molecular structure is not stable and disintegrates into pieces of C_4. These C_4 fragments are the starting units for building up the carbon network. At temperatures up to 400 ^{o}C a mainly sp^3 dominated carbon frame is formed. According to the literature, the change from an aliphatic to an aromatic network should take place between 400 and 500 ^{o}C (Morterra & Low 1983).

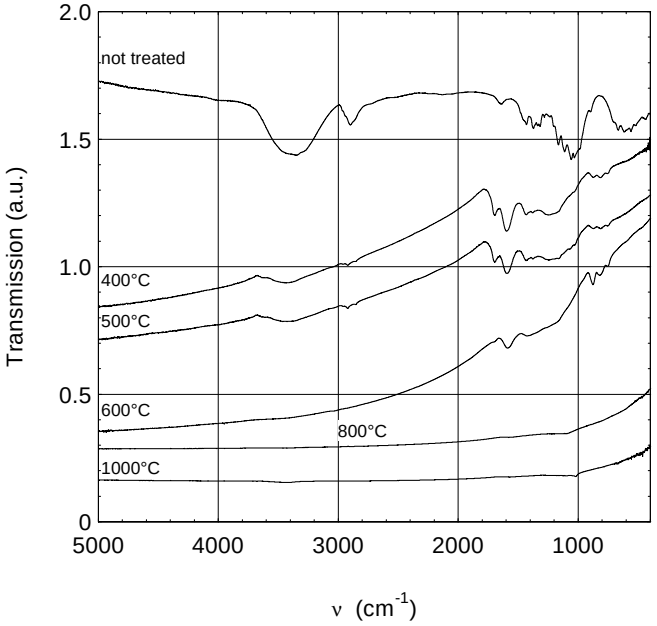

Fig. 1. MIR spectra of non-treated cellulose and cellulose pyrolized at different temperatures. For a better representation the curves have been shifted in the ordinate direction

Table 1. Results of elementary analysis and measured densities of the pyrolyzed cellulose samples

sample name	pyrolysis temperature	(at.%) C	H	O	ϱ (g cm^{-3})
avicel	not treated	28.5	47.7	23.7	1.606
cel 400	400 ^{o}C	56.1	33.3	10.6	1.435
cel 600	600 ^{o}C	72.3	23.9	3.8	1.670
cel 800	800 ^{o}C	85.5	11.9	2.6	1.843
cel 1000	1000 ^{o}C	88.7	8.9	2.4	1.988

Table 1 shows the progress of the carbonization process in the chemical composition of the material determined by combustion elementary analysis. It is obvious that most of the carbonization reactions occur at temperatures up to 600 ^{o}C. The increasing graphitization can be observed by means of the density values which approach the graphitic value of 2.2 g/cm^3 with increasing temperature. The density measurements have been carried out with a Helium-Pycnometer AccupyC 1330 (Fa. Micromeritics).

The carbonization reactions are reflected in detail by infrared transmission spectra (Fig. 1) which have been obtained from ground material dispersed in KBr pellets. Because of the complicated molecular structure of the untreated cellulose its spectrum shows a large number of bands. Their interpretation based on normal coordinate analysis is described in detail in the literature (Cael et al. 1975).

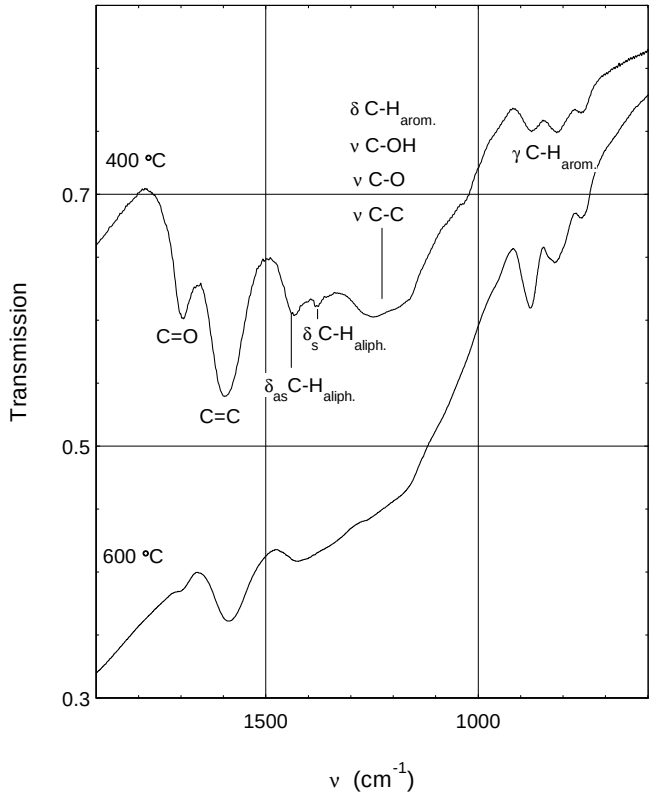

Fig. 2. Enlarged part of the transmission spectrum in the wavenumber region between 600 and 2000 cm^{-1}

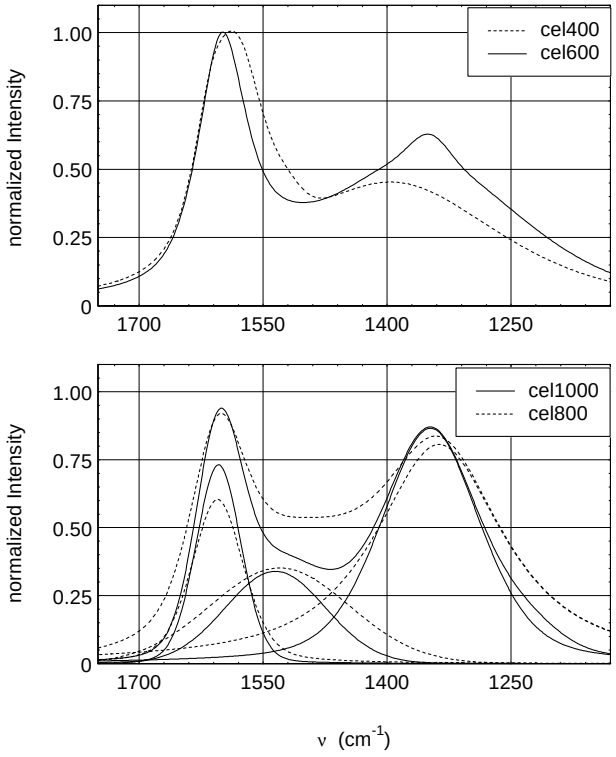

Fig. 3. Raman spectra of pyrolized cellulose

For a better comparison of the measured infrared bands with astronomical spectra the wavenumber region between 600 and 2000 cm^{-1} was enlarged and is shown in Fig. 2. Most of the bands decrease considerably already in the first step of the carbonization process up to 400 °C, for instance the OH- and aliphatic CH-stretching bands at 3390 and 2800–3000 cm^{-1}, respectively. At this temperature, the spectrum exhibits new bands which reflect the presence of degradation products and the combined occurrence of aliphatic and aromatic structural units. For instance, the band at 1705 cm^{-1} is due to alkyl and cycloalkyl ketonic groups expected to be produced during the cellulose degradation. The stronger band at 1595 cm^{-1} is caused by aliphatic or aromatic C=C stretching vibrations which are IR active because of their asymmetric character caused by adjacent ether groups or other oxygen containing groups (Morterra & Low 1983). The weak features at 1430 and 1375 cm^{-1} are assigned to aliphatic CH-deformation vibrations and the broad band between 1100 and 1300 cm^{-1} is caused by C–O stretching vibrations in aliphatic and aromatic ether groups and by C-C stretching vibrations. With increasing temperature, these bands decrease which reflects both the further decomposition of the ketonic compounds to CO and the increasing structural order which reduces the asymmetry of the C=C bonds. In this process, the aromatic part grows continuously. This effect can clearly be observed with the out-of-plane vibrations of aromatic CH groups between 700 and 900 cm^{-1} which increase in strength up to reaction temperatures of 600 °C. The vanishing of this signature in the higher pyrolized cellulose is due to the further loss of hydrogen during the pyrolysis. Most of the functional groups disappeared when 800 °C are reached. The remaining carbon network has no IR-active vibrations. Therefore, its absorption behaviour is dominated by the presence of free charge carriers.

3. Structural characterization of the pyrolysis products

3.1. Raman spectroscopy

The Raman measurements were performed by means of a Jobin-Yvon U1000 Raman system using an Ar-Laser (wavelength 514 nm) for excitation. To avoid an annealing and chemical processing of the strongly absorbing samples, the laser beam was not focused onto the sample. The Raman spectra were recorded in the spectral range between 900 and 2000 cm^{-1} Stokes Raman shift. The results are shown in Fig. 3. A strong fluorescence background decreasing with increasing temperature has been measured for all samples. In Fig. 3 it is already removed by subtraction of a linear function of the wavenumber. Fluorescence is typical for hydrogen-containing carbon materials with a high concentration of sp^3 carbon and a relatively large electronic band gap. It is caused by the radiative recombination of electron-hole pairs produced by the laser irradiation. The falling photoluminescence intensity indicates an increasing efficieny of non-radiative energy dissipation (thermalization) processes

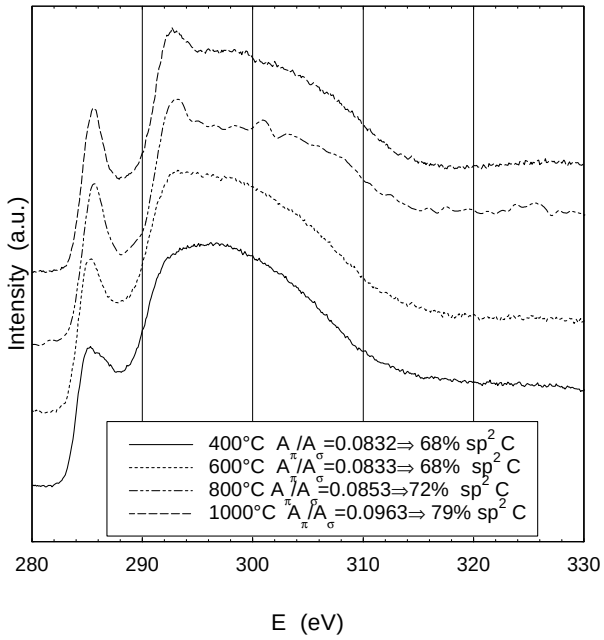

Fig. 4. EEL spectra (core loss) of pyrolized cellulose. The curves are shifted in the ordinate direction

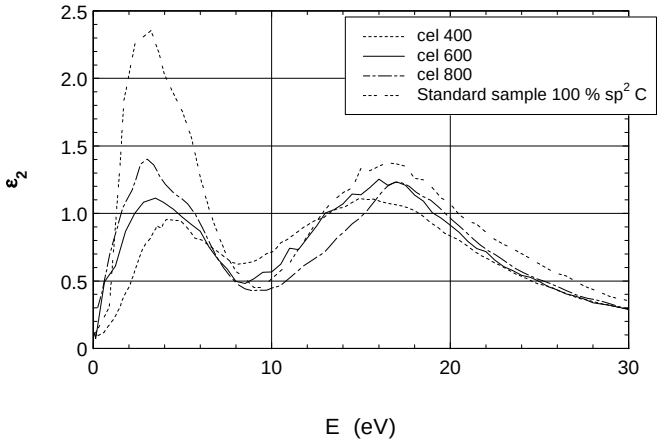

Fig. 5. Imaginary parts of the dielectric functions in contrast to the standard sample with 100 % sp^2 hybridized carbon, evaluated from the EEL spectra (low loss) of pyrolized cellulose.

which require the presence of a large density of gap states provided by the formation of a disordered aromatic network.

Microcrystalline graphite material shows two typical bands in the first order spectrum. The so called G-mode is located at 1580 cm^{-1} and can be assigned to C=C stretching vibrations E_{2g2} of graphite. A second line at about 1350 cm^{-1} corresponds to an A_1-type mode which becomes Raman active in microcrystalline graphite material only (Tuinstra & Koenig 1970; Nemanich et al. 1988; Lespade et al. 1982) (disorder or D-mode). In this case the lack of the long-range translation symmetry causes a breakdown of the momentum conservation rule. A third band between 1500 and 1530 cm^{-1} can be assigned to an amorphous graphite component (Nistor et al. 1994; Huong 1993). The ratio of the integral intensities of the D- and G-lines can be used to determine the crystallite size of the graphitic crystallites in the plane (L_a) (Nistor et al. 1994; Tuinstra & Koenig 1970) as long as no curved structures are present.

For the low-temperature pyrolized samples, the interpretation is not as simple as in the case of the rather graphitic material. The spectra of the cel 400 sample is still dominated by functional group features and vibrations of nongraphitic C=C bonds influenced by adjacent oxygen atoms. In the cel 600 sample most of the functional groups disappeared, but the graphitic domains are still small and strongly disturbed (see the TEM results). The Raman bands in these two samples cannot only be attributed to very small graphitic regions, but also to an overlay of aromatic and aliphatic C=C-bondings in the region between 1580 and 1600 cm^{-1}, and in the 1350 cm^{-1} range by C–C-, C–O–C- and C–OH-bondings. That is why a deconvolution of the cel 400 and cel 600 spectra in the typical graphitic lines is not possible and would provide wrong results for crystallite sizes (L_a) in the plane.

The deconvolution of the other both cellulose spectra was performed in the same way proposed by different authors (Nistor et al. 1994; Nemanich et al. 1988). The spectra of cel 800 and cel 1000 show, that the width of the G- and D-line becomes smaller and the background due to the amorphous part in the spectrum decreases with the higher reaction temperature. The crystallite size L_a increases from 12.8 Å for cel 800 to 16 Å for the cel 1000 sample. The amorphous sp^2 component decreases from 24 % to 20 % for the higher pyrolized sample.

3.2. Electron energy loss spectroscopy and HRTEM

Electron energy loss spectroscopy (EELS) was performed using a Gatan imaging filter (GIF 678) attached to a TEM/STEM Philips CM 200 FEG, run at 200 keV. The energy resolution was about 1 eV. High-resolution transmission electron microscopy (HRTEM) with the CM 200 FEG microscope was performed for sample characterization.

The aim of this kind of spectroscopy was to obtain more quantitative results on the structural changes especially on the hybridization states and the content of sp^3 carbon atoms in the differently carbonized samples . Two energy regions can be used for analysis, first the low-loss region up to 60 eV, where interband transitions and plasmon excitations can be seen and second the core loss region in the range 280-330 eV. The core loss spectra are characterized by the excitations of electrons from the carbon 1s orbital to states above the Fermi level. Fig. 4 shows the carbon K-edge spectra of the differently pyrolized carbon materials. The smaller peak at 285 eV is caused by 1s-π^* transitions and the second one represent the 1s–σ^* transitions. The intensities of the peaks are proportional to the density of states (DOS) in the conduction band. One can immediately see an increase of the π peak in relation to the σ peak and a narrowing of the π peak with increasing carbonization temperature of the sample. In the least carbonized spectrum of cel 400, the

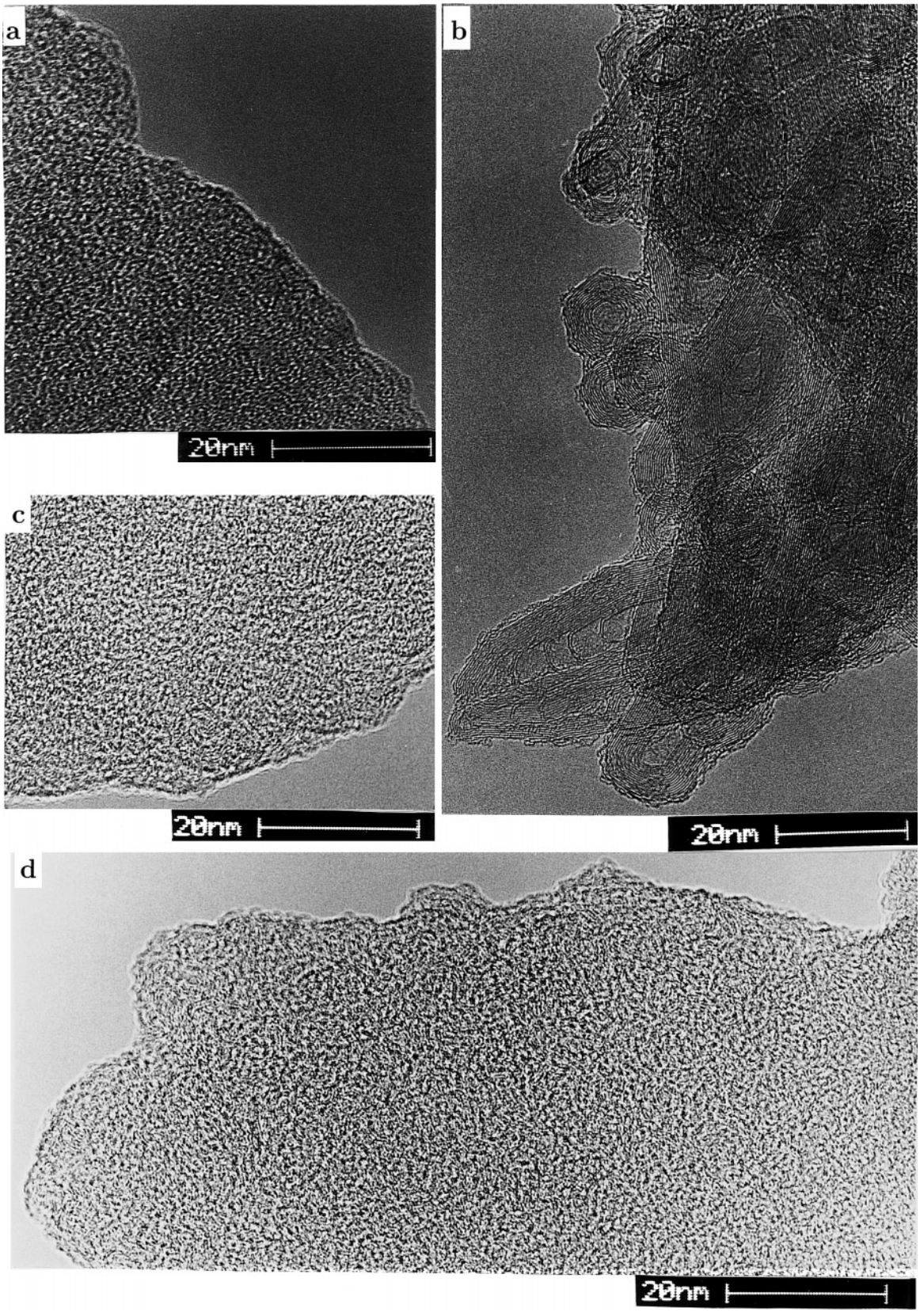

Fig. 6a–d. HRTEM images of at different temperatures pyrolized cellulose. **a** and **b** cel 400, **c** cel 600, **d** cel 1000

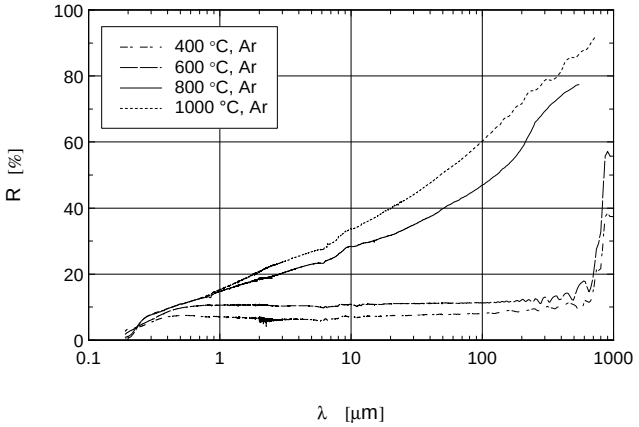

Fig. 7. Reflection spectra of pyrolized cellulose

Table 2. Quantitative content of sp^2 hybridized carbon atoms in the pyrolized cellulose sample, determined with EELS in the core-loss and the low-loss region. The first column contains the name of the samples. The number means the temperature during pyrolisis.

	sp^2 hybrid. C-atoms (%)	
sample	Core Loss	Low Loss
cel 400	68	66
cel 600	68	71
cel 800	72	78
cel 1000	79	81
standard material	100	100

π peak is much broader and seems to have a shoulder between the π and the σ peak. There are different interpretations for the origin of this additional peak between the 1s–π^* and 1s–σ^* transitions. One possibility is the presence of C=O or C≡C bondings in the sample which should have π^* bands lying in the range between 286-288 eV (Bruley et al. 1990). C=O groups are clearly present, but there is no evidence for C≡C bondings from the C–H stretching region of the IR spectrum . The C=O groups probably enhance the determined sp^2 carbon content in the sample, which result in only a small difference in the sp^2 content of the samples cel 400 and cel 600. Another interpretation is that cage-strained π electrons present in bent graphitic layers could provide 1s-π^* electronic transitions in this energy range. Small nanotubes with high curvature radius show such shoulders in contrast to large nanotubes (Ajayan et al. 1993). At carbonization temperatures of 800 and 1000 °C a prominent maximum at about 292 eV is the evidence for the formation of graphite clusters consisting of flat 6-membered rings larger than 1.5 nm (Muller et al. 1993). The intensity ratio of the 1s-π^* and the 1s-σ^* band in the spectra can be used for the quantitative analysis of the sp^2/sp^3 hybridized carbon ratio (Bruley et al. 1994; Fink et al. 1983). Necessary for this kind of analysis is, however, the use of a standard material with a well-known hybridization ratio. For this purpose, we took a graphitic material with microcrystallites in different orientations. The results of the analysis are presented in Table 2.

The second column shows the results of the low-loss spectra of pyrolized cellulose. To extract the loss function from the measured low-loss spectra the zero-loss peak was removed by using a spline fit and following subtraction. The shape of the resulting low energy tail of the low-loss function was again corrected by using the dielectric function of the same materials obtained from optical spectroscopy. For the calculation of the quantitative content of sp^2 hybridized carbon we used the method described by Fink et al. 1984. A Kramers-Kronig analysis was applied to derive the dielectric functions. The loss function was scaled by using the optical data determined by reflection measurements (see the next paragraph). The values of the imaginary part of the dielectric function of the different cellulose low-loss spectra obtained this way are shown in Fig. 5.

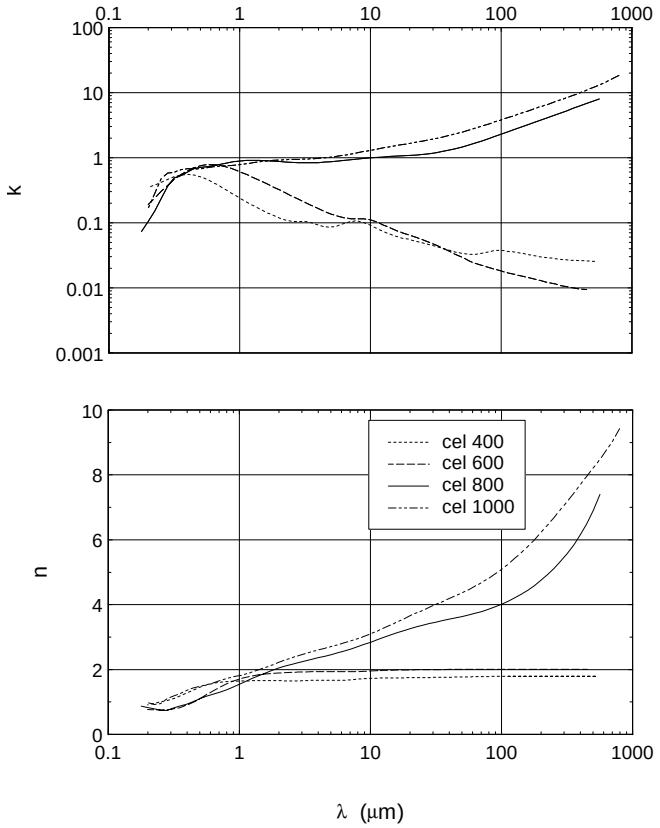

Fig. 8. Optical data of pyrolized cellulose samples.

Using the sum rule

$$N_{eff} = \frac{m}{2\pi^2 e^2 N} \int_0^{E_c} E\epsilon_2(E)dE \qquad (1)$$

N_{eff}: Number of electrons per atom
m:electronic mass
N:density of atoms
ϵ_2:imagenary part of the dielectric function

the effective number of π and σ electrons can be determined. An integration up to E_c = 8 eV provides the number of π-electrons and integration up to E_c = 40 eV gives the number of π- and σ-electrons together. The calculated yields were related to a ratio measured in a fully graphitized and randomly oriented carbon material. One must be very careful in interpreting the

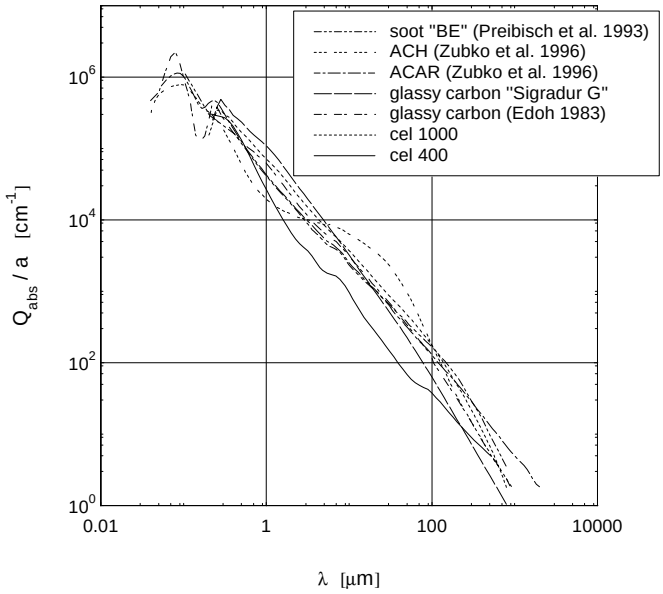

Fig. 9. Absorption efficiency divided by particle radius calculated for spherical particles in vacuum from the optical data of Fig. 8 for pyrolized cellulose materials in contrast to different soot materials and glassy carbon

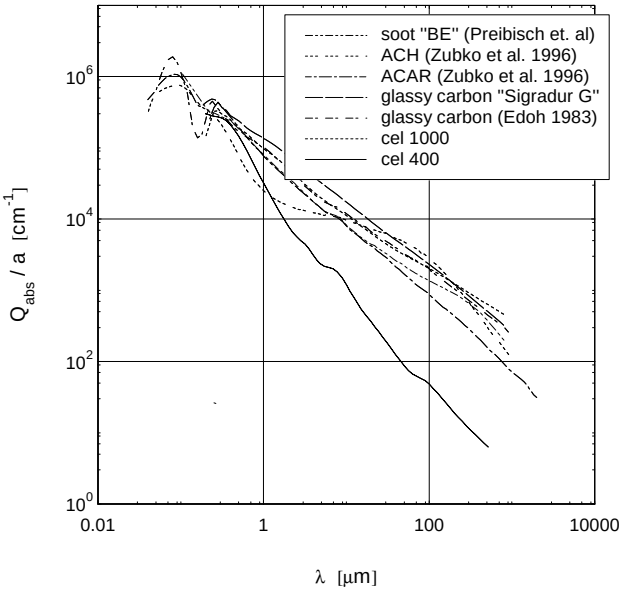

Fig. 10. Absorption efficiency divided by particle radius calculated for a CDE in vacuum from the optical data of Fig. 8 for pyrolized cellulose materials in contrast to different soot materials and glassy carbon

hybridization results. There seem to be only small differences between the differently pyrolized materials (cel 400 and cel 600), but one has to take into acount, that the sp^2 hybridized carbon in the 400 and 600 °C treated sample consists of more aliphatic than aromatic structures. In addition, C=O groups exist which increase the content of sp^2 carbon. Drastic changes in the structures take place between 600 and 800 °C very well seen in the increase of the reflectance (see Fig. 7) and the changes in the core-loss spectra. Structural changes are also visible in the HRTEM images (Fig. 6).

The main structure seen in the sample cel 400 is amorphous (≡ no structural units seen by HRTEM, see Fig. 6a). Surprisingly, onion-like particles and small nanotubes could be seen by HRTEM (Fig. 6b) in case of the cel 400 sample. The quantitative amount of this kind of particles is determined with not more than a few percent. Usually one needs temperatures of more than 2000 °C to form onion-like particles and nanotubes. Furthermore all other samples do not show these structures. That is why we assume that a catalytic process could be responsible for the synthesis of these particles.

Small graphitic crystallites embedded in an amorphous structure can be seen in Fig. 6c of cel 600. The distance between the graphitic layers is still much higher than the expected value of 0.335 nm in graphite and is about 0.4 nm. The layers are often tilted to each other.

Larger graphite crystallites are present in the sample cel 1000 (Fig. 6d). The average size of the crystallites is about 2 nm. The distances between the graphite layers is smaller than in the cel 600 sample and could be determined with about 0.37 nm. In general the crystallites are randomly oriented. This is the result of the original tangled polymer structure which influences strongly the structure of the pyrolysis products. A more ordered material with graphitic ranges up to about 40 nm would be expected at higher pyrolysis temperatures where, however, the tangled structure is still maintained. This kind of material is called glassy carbon.

3.3. Spectroscopy of bulk samples

For the spectroscopic characterization of the materials in the ultraviolet, visible, and infrared regions of the electromagnetic spectrum, the reflectance of the bulk samples in the 0.2–500 μm wavelength range has been measured by means of two spectrometers (Bruker FTIR 113v and Perkin Elmer Lambda 19) equipped with standard accessories for specular reflectance measurements at near-normal incidence. The reflection spectra (Fig. 7) show a remarkable change in the general behaviour of the infrared reflectance occuring between 600 and 800 °C annealing temperature.

At the lower pyrolysis temperatures, the reflectance is nearly constant from the visible throughout the infrared which indicates that there is no strong absorption process influencing the spectral behaviour in this region. At very long wavelengths, a sinusoidal structure occurs which indicates that the sample becomes partly transparent at these wavelengths and allows the interference of beam portions reflected at both interfaces of the sample. The strong rise of the reflectivity at about 300 μm is also a result of these interferences. In contrast to this behaviour which is characteristic for a insulator or semiconductor, the reflectance of the 800 °C and 1000 °C samples increases continuously throughout the infrared. This is characteristic for a material with a large number of free charge carriers.

The reflectance spectra offer the possibility to calculate the complex refractive index $m = n + ik$ (optical data) of the material by a Lorentz oscillator fit method. The interference region in the spectra of the lower-temperature samples has to be omitted in this calculation. The reason is that the interferences cannot be modelled accurately because the exact sample geometry is unknown due to the polishing process. However, the transparency of the samples in this region allows us to measure the absorbance (optical depth) of the material in the far infrared by a transmission experiment. For this purpose, ultrathin sections (≈ 60 μm thickness) of the cel 400 and cel 600 materials have been prepared. The analogous thin sections prepared from the other materials have not been transparent. The reflection losses at the two interfaces, which have been extrapolated from the reflectance measurements in the middle IR, were taken into account. From the resulting absorbance, the imaginary part k of the refractive index could be calculated directly.

4. Optical data and astrophysical application

The combined results in terms of the optical data n and k are shown in Fig. 8[1]. Significant differences in the behaviour of the n- and k-values can be seen between the low-temperature samples (cel 400, cel 600) and the high-temperature materials (cel 800, cel 1000). The low-temperature samples show an increase of n up to 1 μm and a constant value in the IR. The imaginary part k first increases and begins to decrease at about 1μm up to 500 μm. The n- and k-data of the cel 600 sample are higher in comparison to the cel 400 sample, which originates from the higher content of sp^2 hybridized carbon atoms and the beginning of aromatization processes in this sample. The two high-temperature samples show an increase of n and k from 200 nm to 500 μm, similar to the optical data of glassy carbon.

The previous calculations of the optical constants for soot material, performed by different authors (Zubko et al. 1996; Preibisch et al. 1993) are based on extinction measurements with the limitations already mentioned in the introduction. For these calculations a complicated model of the morphology is necessary. Therefore, these methods provide results with large uncertainties, especially in the FIR region. An exact determination of optical constants of soot material is only possible in samples with isolated soot particles, which can be realized in matrix-isolated samples (Schnaiter et al. 1997). In our calculations based on reflectance measurements, the deviation of optical constants is straightforward and precise.

Especially interesting for astronomy is the opacity of small grains in vacuum, which can be calculated from the optical constants for spherical shapes by the Mie theory. Shape effects can roughly be simulated by a continous distribution of ellipsoids with the same probability of all shape parameters (CDE) in the Rayleigh limit (Bohren & Huffman 1983). In Figs. 9 and 10 the calculated normalized absorption efficiencies of cel 400 and cel 1000 are compared with those of glassy carbon "Sigradur G" (Fa. Hochtemperatur-Werkstoffe GmbH, temperature treatment 3000 °C) measured in our laboratory and glassy carbon measured by Edoh (1983) and of amorphous carbon soot (Zubko et al. 1996; Preibisch et al. 1993) and hydrogen containing soot (Zubko et al. 1996).

[1] The n- and k-data files can be taken from the internet homepage of the Astrophysical Institute and University Observatory Jena (http://www.astro.uni-jena.de).

Table 3. Calculated spectral indices in the FIR ($\lambda \geq 100\mu m$) of different pyrolized cellulose materials for spheres and CDE

	spectral Index β for $\lambda \geq 100\mu m$	
sample	Spheres	CDE
cel 400	1.25	1.25
cel 600	1.50	1.50
cel 800	1.95	0.69
cel 1000	2.28	0.71

We have shown that it is important to document the influence of different carbon structures on the optical properties, not only in the UV region but also at the FIR wavelengths. Since we do not yet know the predominant carbon structure in space, the necessity of exact optical constants of carbon materials with larger differences in structure is very important. They offer the possibility to perform radiative transport calculations and to develop new dust models on the basis of differently structured carbon.

The normalized absorption efficiency of carbonaceous particles in the FIR follows a power law ($Q_{abs}/a \sim \lambda^{-\beta}$). The spectral index β depends strongly on the internal structure of the carbon materials. A well-ordered graphitic material should provide a spectral index of about 2 for spheres, whereas a less ordered amorphous structure shows a lower value for β of about 1 (Preibisch et al. 1993; Henning et al. 1995). The results of our calculation for spheres and the CDE are given in Table 3.

In Fig. 9 the strongly disorderd material cel 400 shows a smaller absorption efficiency in the wavelength region between 0.6 and 100 μm of the order of 3 magnitudes compared to the other carbon materials. The spectral index β in the long wavelength tail is considerably lower than the exponents of the other carbon materials. From Table 3 it is clear that there is a gradual increase of β for spherical grains with increasing graphitization in the pyrolyzed cellulose materials. This increase ranges indeed from about 1 to about 2 as predicted by theory. The samples pyrolized at higher temperature (cel 1000) with their graphite-like structures behave similar to glassy carbon.

Our CDE calculations show that there is no strong morphological effect on the spectral index for the low-temperature samples in contrast to the more graphitic materials where we find a considerably lower index. The latter is caused by percolation effects, present in the more graphitized samples which contain free charge carriers. In case of conducting materials (such as graphite), an increase of the FIR opacity and a flatter curve of absorptivity are theoretically expected for aggregated particles or deviations of the shape of particles from a sphere (Stognienko et al. 1995; Henning et al. 1995). We should caution the reader that the results of the CDE calculations serve only as an illustrative example. For a more realistic calculation, one has

to assume a special aggregate structure and/or shape distribution of the individual particles (see Stognienko et al. 1995). For extreme values of the refractive indices, computational methods for the calculation of the absorption by aggregates or elongated particles meet their limits (Michel et al. 1996). For a detailed discussion of the relation between observationally-based FIR opacities and laboratory measurements we refer the reader to the review paper by Henning et al. (1995).

5. Conclusion

The synthesis of bulk carbon samples with different structures and ratios of sp^2 to sp^3 hybridized carbon and the determination of optical constants from reflection spectra provides the possibility to investigate the influence of the structure on the optical properties independent of the shape, size and agglomeration state of carbon particles. The main point of this work was the exact structural characterization of the carbonized cellulose samples. Very effective methods to characterize carbon structures are HRTEM and EELS spectroscopy which gives quantitative results on the hybridization state of the carbon atoms. The sample pyrolized at 400 °C is dominated by an aliphatic structure. The content of sp^2 hybridized carbon is about 66 %. The transition from aliphatic to aromatic structural elements happens between 400 and 600 °C. The dimensions of the graphitic regions at 600 °C are still very small and the distances between the graphite layers are too large for regular graphite. The layers are twisted and shifted to each other. These graphitic regions are embedded in an amorphous matrix. The content of sp^2 hybridized carbon is about 71 %. The spectra of both materials are very similar and they are typical for a non-conducting material. The exponent of the power law in the FIR is increased compared to the cel 400 sample, which is caused by the higher sp^2/sp^3 hybridization ratio and the change from the more aliphatic to the aromatic structure.

A considerable change in structure and optical properties takes place between 600 and 800 °C, when more ordered graphitic regions with an average size of about 1.5 nm are formed in the carbonized samples. The optical behaviour of this material is completely different compared to the low-temperature samples. The transmission spectra become structureless and the optical constants show a continuous rise from the UV to the FIR, which is caused by free charge carriers. The calculation of the normalized absorption efficiency from the optical constants shows that the spectral index β in the long-wavelength tail increases with the enhancement of the content of sp^2 hybridized carbon and with increasing structural order. In the high graphitized samples cel 800 and cel 1000 there is a dependence of the spectral index β on the morphology of the carbon sample. Morphological effects like agglomeration lead to a strong decrease of β compared to spherical grains, which can be seen in the CDE calculations.

Acknowledgements. We wish to thank Prof. Schlögl from the Fritz-Haber-Institute of the Max-Planck-Society for the possibility to use the HRTEM and EELS and especially Dr. Spillecke for the help with the measurements. This work was partly supported by a grant from the Max-Planck-Society to T.H., which includes H.M. participation in this project.

References

Ajayan P.M., Iijima S., Ichihashi T. 1993, Physical Review B, 47(11), 6859
Bohren C.F., Huffman D.R. 1983, Absorption and Scattering of Light by Small Particles, John Wiley and Sons, New York
Bruley J., Madakson P., Liu J.C. 1990, Nuclear Instruments and Methods in Physics Research, B45, 618
Bruley J., Williams D.B., Zhang Z. 1994, ICEM,Paris, 13
Cael J.J., Gardner K.H., Koenig J.L., Blackwell J. 1975, J. Chem. Phys., 62, 1145
Campbell M.F., Elias J.H., Gezari D.Y., et al. 1976, ApJ, 208, 396
Draine B.T., Lee H.M. 1984, ApJ, 285, 89
Edoh O. 1983, Dissertation, University of Arizona
Fink J., Müller-Heinzerling T., Bubenzer A., Koidl P., Crecelius G. 1983, Solid State Communications, 47, 687
Fink J., Müller-Heinzerling Th., Pflüger J., et al. 1984, Physical Review B, 30(8), 4713
Gürtler J., Kömpe C., Henning Th. 1996, A&A, 305, 878
Henning Th., Michel B., Stognienko R. 1995, Planet. Space Sci., 213, 1333
Huong P.V. 1993, Journal of Molecular Structure, 292, 81
Kittel C. 1963, Introduction to Solid State Physics, John Wiley, New York
Koike C., Kimura S., Kaito C., et al. 1995, ApJ, 446, 902
Lespade P., Al-Jishi R., Dresselhaus M.S. 1982, Carbon, 20, 427
Li A., Greenberg M. 1997, A&A, submitted
Martin P.G., Rogers C. 1987, ApJ, 322, 374
Menella V., Colangeli L., Bussoletti E. 1995, A&A, 295, 165
Michel B., Henning Th., Stognienko R., Rouleau F. 1996, ApJ, 468, 834
Morterra C., Low M.J.D. 1983, Carbon, 21, 283
Muller D.A., Tzou Y., Raj R., Silcox J. 1993, Material Research Society Symposium Proceedings, No. 164, MRS, Pittsburgh
Nemanich R.J., Glass J.T., Lucovsky G., Shroder R.E. 1988, J. Vac. Sci. Technol., A6, 1783
Nistor L.C., Van Landuyt J., Ralchenko V.G., et al. 1994, Applied Physics, A58, 137
Otani S., Oya A. 1991, in R.W. Cahn, P. Haasen, and E.J. Kramer (eds.), Glasses and amorphous materials, pp 549–572, VCH, Weinheim
Papoular R., Conard J., Guillois O., et al. 1996, A&A, 315, 222
Preibisch Th., Ossenkopf V., Yorke H. W., Henning Th. 1993, A&A, 279, 577
Rouleau F., Martin P.G. 1991, ApJ, 377, 526
Schnaiter M., Mutschke H., Henning Th., Dorschner J., Salama F. 1997, ApJ, submitted
Sopka R.J., Hildebrand R.H., Jaffe D.T., et al. 1985, ApJ, 294, 242
Stognienko R., Henning Th., Ossenkopf V. 1995, A&A, 296, 797
Tang M.M., Bacon R. 1964, Carbon, 2, 211
Tuinstra F., Koenig J.L. 1970, J. Chem. Phys., 53, 1126
Zubko V.G., Menella V., Colangeli L., Bussoletti E. 1996, MNRAS, 282, 1321

This article was processed by the author using Springer-Verlag LaTeX A&A style file *L-AA* version 3.